ELSEVIER

Journal of Alloys and Compounds 300–301 (2000) 199–206

Journal of ALLOYS AND COMPOUNDS

www.elsevier.com/locate/jallcom

Radiative recombination in Ce-, Pr-, and Tb-doped barium fluoride

Andrzej J. Wojtowicz[a,b,*], Piotr Szupryczynski[a,b], Winicjusz Drozdowski[a]

[a] *Institute of Physics, N. Copernicus University, Torun, Poland*
[b] *Chemistry Department, Boston University, Boston, MA, USA*

Abstract

Open f-shell rare-earth ions doped into a solid state matrix often easily change their charge state via interactions with charge carriers generated by ionizing radiation. This feature promotes a desired efficient radiative recombination of separated charge carriers at rare-earth ion sites but it may also help to stabilize various radiation defects that destructively interfere with the scintillation. The well-known effect responsible for scintillation light loss due to absorptions introduced by these so-called 'radiation damage' centers in alkali halides has been identified and studied for a long time. In this communication we concentrate on a different and much less-known and studied effect in which radiation induced centers directly and actively participate in the scintillation process itself. We present and discuss some selected recent results that illustrate the importance of competition between the prompt radiative recombination via rare-earth ions and generation of radiation damage centers in barium fluoride crystals activated with Ce, Pr and Tb. We demonstrate that results of such measurements as radioluminescence spectra, VUV spectroscopy, low temperature thermoluminescence glow curves, isothermal decays, and scintillation time profiles can be consistently explained in the frame of a simple model that includes one recombination center (RE ion) and a number of charge traps. We find that the trap model of radiation damage centers such as V_k centers describes reasonably well their participation in the scintillation process that includes creation (equivalent to charge carrier trapping) and thermally activated decomposition (charge carrier release). These effects are shown to account quantitatively for important characteristics of the scintillation process such as large variations in the scintillation light yield with temperature and longer decay times in the scintillation time profiles that effectively lower the scintillation light yield at ambient temperatures.

Keywords: Radiation effects, Recombination and trapping; Luminescence; Synchrotron radiation; Thermal analysis

1. Introduction

Since in the process of radioluminescence and/or scintillation the energy deposited in the host material by ionizing radiation must be extracted by recombination of electron-hole pairs, deep traps have long been suspected to reduce the scintillation light yield of any scintillator material [1].

It has been recently suggested that also relatively shallow traps may be responsible for the previously unexplained large variations of the scintillation light yield with temperature leading to lower scintillation light output at ambient temperatures [2]. In particular measurements of the thermoluminescence glow curve (TL) and the scintillation light yield against temperature (LY vs. T) on the two Ce-activated scintillator materials, $LuAlO_3$ (LuAP) and $YAlO_3$ (YAP), have been found very instructive [3]. The results of these two experiments, interpreted in the frame of a simple one-recombination center and one-trap model of first order kinetics, provide trap parameters that not only reproduce reasonably well the TL and LY vs. T curves but are also consistent with the scintillation time profiles measured at room temperature [4].

In a different approach the measurements of the low temperature thermoluminescence (ltTL), isothermal decays (ITD) and scintillation time profiles (STP), were used to extract the parameters of shallow traps that actively participate in the scintillation process in the Ce-activated BaF_2 [5]. These results have been later augmented by the VUV spectroscopy, spectrally resolved TL, and time profile measurements under synchrotron excitation [6]. The conclusion of that work was that, contrary to earlier suggestions [7], the dominant light producing mechanism in BaF_2:Ce under ionizing excitation is due to the charge carrier recombination at the Ce^{3+}-sites and not to the energy transfer from the self-trapped excitons.

It has also been demonstrated that radiative recombination via Ce^{3+} ions in BaF_2 involves two different channels [6]. The first one, responsible for the direct scintillation

*Corresponding author. Tel.: +48-56-210-65; fax: +48-56-253-97.
E-mail address: andywojt@phys.uni.torum.pl (A.J. Wojtowicz)

0925-8388/00/$ – see front matter
PII: S0925-8388(99)00723-9

component with no rise time and decay of about 30 ns (the Ce^{3+} radiative lifetime), involves recombination of electrons and those Ce^{4+} that have previously captured the initially generated holes. The second channel is due to recombination of mobile self-trapped holes and Ce^{2+} ions (and/or the so-called PC centers [8]), that have captured the initially generated electrons. It is the thermally activated release of holes trapped at various sites (V_k, H, V_{kA}) that introduces all the 'trap-related' features, resembling those observed in LuAP–Ce and YAP–Ce, to the scintillation process in BaF_2 [5,6]. Although some participation of excitonic energy transfer mechanism can not be excluded the final conclusion of this work was that the dominant mechanism of light production in BaF_2 under ionizing excitation must involve radiative recombination of charge carriers, electrons and holes (mobile V_k centers) at the Ce^{3+} ion sites.

In this communication we report results of measurements of radioluminescence spectra, VUV excited luminescence spectra, luminescence excitation spectra and decays, ltTL, ITD, STP and LY vs. *T* of BaF_2 activated with Ce, Pr and Tb. We will analyze and interpret these results in the frame of the same recombination model that was earlier applied to the Ce-activated BaF_2 [5,6].

2. Crystals and experimental procedures

The crystals of undoped BaF_2, BaF_2:Tb, BaF_2:Pr, BaF_2:Ce were grown by Optovac (North Brookfield, MA, USA) using the Bridgman method. The concentrations of rare earths in the melt were 0.2 mol% for each of the doped crystals. The individual samples were of high optical quality, clear, displayed no color and no indication of oxygen contamination, and were not subjected to any chemical reducing procedure.

The steady state radioluminescence spectra were recorded at room temperature using a standard set-up consisting of an X-ray tube operated continuously at 35 kV and 25 mA, a monochromator (Acton Research SpectraPro-500) and a photomultiplier (Hamamatsu R928). The experiment was controlled by a PC computer. The spectra were not corrected for the spectral sensitivity of the system.

The VUV experiments (luminescence and excitation spectra, pulsed VUV-excited emission time profiles) were conducted at the SUPERLUMI station of HASYLAB, Hamburg, Germany. A detailed description of SUPERLUMI's experimental facilities was given by Zimmerer [9] and is also available on-line [10].

The ltTL glow curves were measured using a closed-cycle double compressor He cooler with a programmable heater. Prior to TL runs the samples were irradiated for about 20 h by an X-ray source (Am^{241}) at 4 K. During TL runs the heating rate was kept constant at 9 K/min. The ITD experiments were performed using a different heating cycle; the sample was irradiated at 4 K and then the temperature was raised to some predetermined higher value and held there for an appropriate time up to 3000 s during which the intensity of emission released from the sample was measured and recorded against time.

The scintillation time profiles were measured at selected temperatures using a set-up based on a standard closed-cycle He cooler with a sample chamber adapted to accommodate a γ-radioactive source (Ru^{106}). A standard synchronous photon counting method was used to record time profiles of γ-excited emission pulses. The temperature of the sample was controlled by a temperature controller in the range of 20–350 K. The same set-up was used to measure scintillation light yields against temperature. The radioactive source used in this experiment was Cs^{137}. A more detailed description of the light yield measurements is given in Ref. [3].

3. Results and discussion

3.1. Radioluminescence

Unlike photoluminescence spectra that often correspond to only one specific excitation channel selected by the excitation light wavelength, radioluminescence spectra usually reflect the dominant radiative decay mode of elementary electronic excitations of the host material, electron-hole pairs and/or excitons, generated by γ- or X-radiations.

The radioluminescence spectra shown in Fig. 1 show, nevertheless, all kinds of emissions that are expected from rare earth activated BaF_2 [8]. The undoped sample (Fig. 1a) shows the two well known broad bands peaking at about 300 and 220 nm that correspond to radiative decay of self-trapped excitons (the STE band at 300 nm [11]), and the so-called core-valence luminescence (the CVL band at 220 nm) characteristic for the radiative recombination of core holes and valence band electrons. The Ce-doped sample (Fig. 1b) shows a well known double band characteristic for the d–f transition at the Ce^{3+} ion, but there are also some Ce-absorption distorted remnants of the STE emission band. This observation indicates that at least part of the total energy deposited in the crystal by ionizing radiation decays radiatively via STE decay. A large overlap between the STE emission and Ce-absorption bands seems also to suggest that radiative and non-radiative energy transfer from STE to Ce-ions is possible and may play a role, as suggested earlier by Visser et al. [7].

The radioluminescence spectrum of BaF_2:Pr (Fig. 1c) is clearly the most interesting one as it shows all of the possible emissions. The spectrum displays a large and rather undistorted STE band at 300 nm, there are present the well known d–f emission bands between 220 and 290 nm, and, eventually, there also is a set of f–f emission lines in the range between 460 and 500 nm. Some

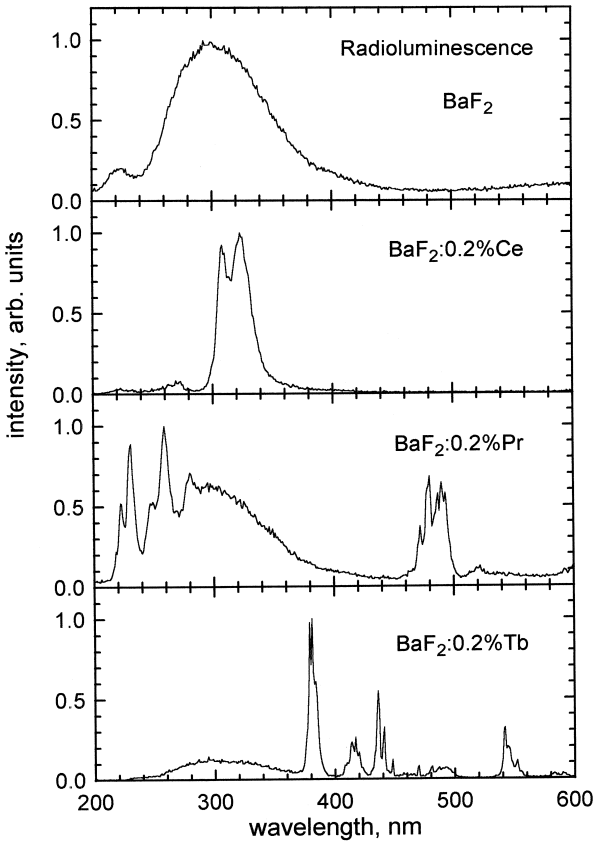

Fig. 1. Radioluminescence spectra of BaF_2 (a), BaF_2–Ce (b), BaF_2–Pr (c) and BaF_2–Tb (d) at room temperature. The samples were excited by X-rays from the X-ray tube operated continuously at 35 kV and 25 mA. Note the presence of the STE emission band at 300 nm. Both d–f and f–f emissions are present under ionizing irradiation for all of the ions studied. The spectra were not corrected for spectral sensitivity of the set-up.

contribution of the CVL band at 220 nm may also be present as the f–d absorption bands do not extend too much beyond 220 nm. Clearly the STE emission and Pr absorption bands do not overlap and the STE-Pr^{3+} energy transfer is not very likely to provide a dominant radioluminescence mechanism in the Pr-activated BaF_2.

The radioluminescence spectrum of the Tb-activated BaF_2, shown in Fig. 1d, shows a large contribution of f–f emission lines, a weaker STE band and probably some of the CVL band. The f–d absorption bands are, most likely, positioned at the wavelengths not longer than, say, about 230 nm. It is very likely that the d–f emission bands are quenched via non-radiative energy transfer to higher lying f–f levels since the shortest wavelength f–f emission line of Tb^{3+} is positioned at about 380 nm, instead of 470 nm as in the BaF_2:Pr. And again, there is no indication of any significant overlap between the STE and Tb^{3+} f–f absorption bands that would point to the STE-Tb^{3+} energy transfer as the important mechanism of radioluminescence in BaF_2:Tb. Let us note that the relative contribution of the 3+ ion emission in BaF_2:Tb to the total steady state radioluminescence is certainly higher than in BaF_2:Pr although not as high as in the case of BaF_2:Ce.

3.2. VUV spectroscopy

Although some initial results of synchrotron VUV experiments have already been presented in Ref. [6] a full account of this work requires that additional experiments must be performed. Consequently we limit our presentation here to selected results obtained on BaF_2:Ce.

The VUV excited luminescence and luminescence excitation spectra covering UV and VUV spectral ranges of d–f and f–d transitions of Ce^{3+} ions in BaF_2:Ce are shown in Fig. 2. We note that under the VUV excitation the emission spectrum shows almost exclusively the Ce^{3+} emission with practically no contribution from the STE band. Nevertheless the emission time profiles for the two excitations, at the wavelengths of 60 and 75 nm, shown in Fig. 3, are very different, with the higher photon energy excited profile showing much faster decay with the Ce^{3+} radiative lifetime of about 30 ns. The explanation of this effect was proposed by Wojtowicz et al. [6]. They note that the 75 nm excitation of lower photon energy falls below, while the 60 nm excitation of higher photon energy falls above the threshold defined by the position of the relevant Ba^{2+} core level involved in the production of the CVL photons. Thus part of the exciting photon energy at the 60 nm excitation is used to produce a CVL photon and, consequently, the electron-hole pairs produced are effectively less separated than in the case of the less energetic 75 nm excitation. It appears therefore that the 'direct' excitation, emulated by a

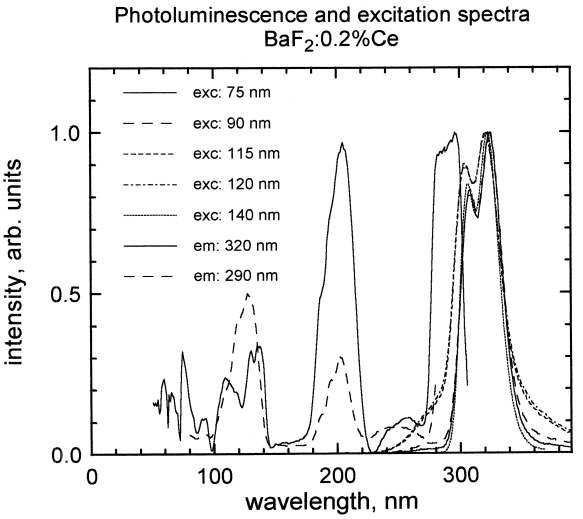

Fig. 2. Luminescence and excitation spectra of BaF_2:Ce at room temperature. Different excitation and emission wavelengths were employed in order to identify different excitation and radiative deexcitation channels. Note that under the VUV excitation the emission spectra show almost no STE contribution. The salicylate standard was used to correct the excitation spectra. The emission spectra were not corrected.

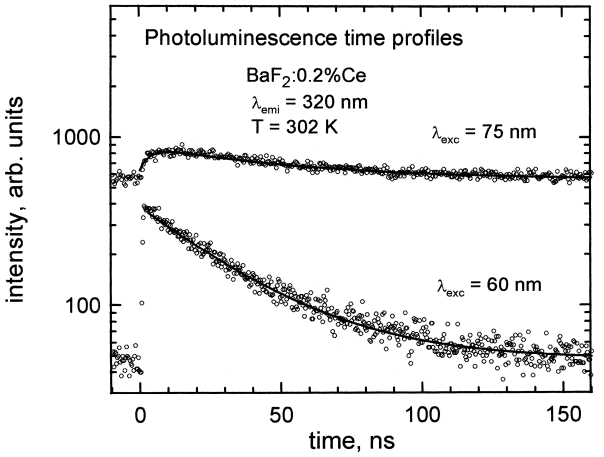

Fig. 3. Photoluminescence time profiles of BaF_2:Ce under 60 and 75 nm excitations by synchrotron pulses at room temperature. Empty circles represent experimental points while solid lines depict three- (75 nm) and one-exponential (60 nm) fits. Note the large pile-up background in the case of the 75 nm excitation and a much faster decay of the emission excited by VUV light of 60 nm wavelength.

60 nm VUV excitation involves, most likely, a prompt hole trapping by the Ce^{3+} ions followed by electron capture and recombination. The 'indirect' slowly decaying component emulated by the 75 nm excitation involves therefore well separated electron-hole pairs that are more likely to be trapped and detrapped before they find each other and recombine.

The solid lines in Fig. 3 present multiexponential fits to the experimental points. The summary of the fit parameters for the 75 nm excitation is given in Table 1.

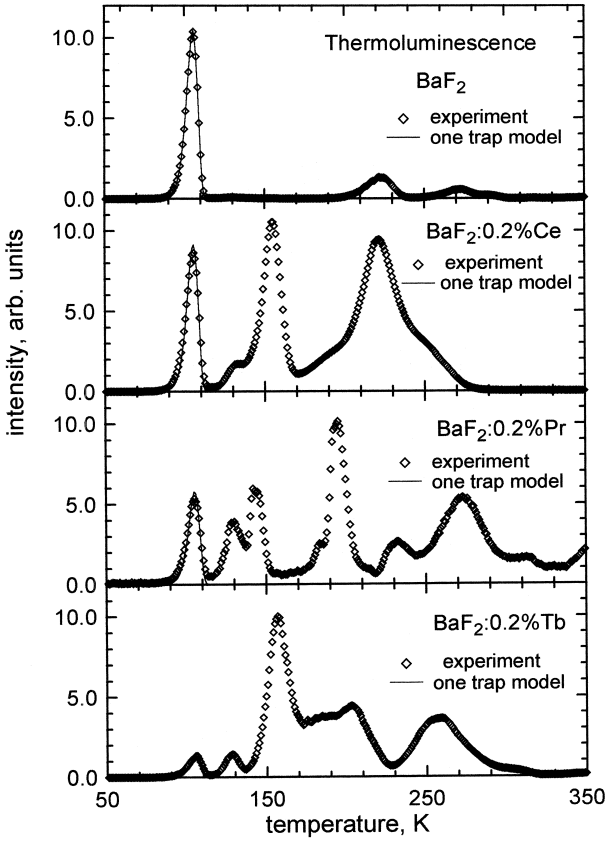

Fig. 4. Thermoluminescence glow curves of BaF_2, BaF_2:Ce, BaF_2:Pr and BaF_2:Tb following X-ray irradiation at 4 K. The heating rate was 9 K/min. Empty circles represent experimental points while solid lines represent calculated curves with parameters derived from the ITD and STP experiments. With exception of shifts to correct for the thermal lag, there is no other adjustable parameter.

3.3. Low temperature thermoluminescence

The ltTL glow curves of undoped, Ce, Pr and Tb doped BaF_2 crystals measured at a heating rate of 9 K/min are shown by experimental points in Fig. 4. While the glow curve of undoped crystal is dominated by a single well developed peak at about 108 K all of the doped crystal curves display additional peaks that are comparable in intensity or even stronger at 135, 159, 170, 225 and 260 K (BaF_2:Ce), 130, 145, 198, 235 and 275 K (BaF_2:Pr), 131, 160, 206, 261 and 305 K (BaF_2:Tb).

Table 1
Summary of the results of the time profile measurements and fits for BaF_2:Ce under pulsed VUV synchrotron excitation at 75 nm[a]

Temp. (K)	y_0	A_1	τ_1 (ns)	A_2	τ_2 (ns)
240.3	0.566	0.418	31.5	0.104	3.26
258.6	0.365	0.278	32.0	0.308	496
280.6	0.546	0.079	32.6	0.325	109
302.0	0.611	0.095	33.1	0.293	64.2
315.7	0.570	0.067	33.5	0.428	41.6

[a] Decay times in ns and zero-time amplitudes in arbitrary units were derived from the three-exponential fits (including the rise time term, not shown) to the experimental points.

In general agreement with previous studies we note that the peak at 108 K, present in both undoped and doped crystals, is most likely due to thermally activated annealing of the so-called V_k-centers (self-trapped holes) while the remaining peaks are most likely due to dissociation or thermal annealing of other defects induced by rare-earth doping [8,11]. In particular the peaks at 130–135 and 145–160 K, present in all of the doped samples, could be due to defects involving interstitial fluorine ions F^{1-} (designated H) that compensate the additional charge of the 3+ rare earth ion substituting for a 2+ cation (Ba^{2+}) [8,11].

The solid lines plotted in Fig. 4 represent calculations that were performed using the Randall and Wilkins formula for first order kinetics [12]:

$$I(T) = n_0 s \exp\left(-\frac{E}{k_B T}\right) \exp\left[-\frac{s}{\beta}\int_{T_0}^{T} \exp\left(\frac{E}{k_B T}\right) \mathrm{d}T\right] \quad (1)$$

where T is the sample temperature, n_0, T_0 are the initial filled trap concentration and the initial temperature, respectively, s stands for the frequency factor, k_B the Boltzman constant, E the trap depth, and β the heating rate. The procedure and experiments from which the trap parameters s and E have been derived will be outlined below. The conventional term 'trap' is used here for simplicity but we are aware of the fact that reality (thermally activated motion and subsequent decay of V_k centers) is far more complex.

3.4. Isothermal decays and scintillation time profiles

The isothermal decays (ITD) have been measured in the range of temperatures covered by the V_k glow peak for all of the samples. Since the results obtained for the undoped and Ce-doped samples have already been published [5] we limit our presentation here to BaF_2:Pr and BaF_2:Tb. In Fig. 5 by experimental points we present representative ITD curves of the Tb doped samples. Two-exponential fits to the experimental points are depicted by solid lines. It appears that the dominant decay constants shorten as the temperature increases. The parameters of the fits obtained for all of the measured ITD curves are summarized in Tables 2 and 3.

In Fig. 6 we present by the experimental points the scintillation time profiles of BaF_2:Pr at selected temperatures to illustrate general trends. The solid lines represent three exponential fits to the experimental points. The parameters of the fits obtained for all of the measured time profiles are summarized in Table 4. We observe that there are two components that are temperature independent; the fast component of about 0.9–1 ns (the CVL band at 220 nm) and the component of 18–20 ns (the Pr^{3+} radiative lifetime). The third component shows some thermally induced variations in the temperature range of 250–300 K.

As already mentioned there is no d–f emission from Tb^{3+} in BaF_2. Therefore scintillation time profiles of BaF_2:Tb are too slow and could not be measured.

Since ITD curves are due to radiative recombination that follows thermally activated release of self-trapped holes their decay constants reflect the effective trap lifetimes t at the predetermined temperatures T described by the following formula:

$$\tau = s^{-1} \exp\left(\frac{E}{k_B T}\right) \tag{2}$$

or, equivalently

$$\ln \tau = \frac{E}{k_B} \cdot \frac{1}{T} - \ln s \tag{3}$$

This last relation can be used to extract the trap parameters, s and E, by plotting the natural log of the measured

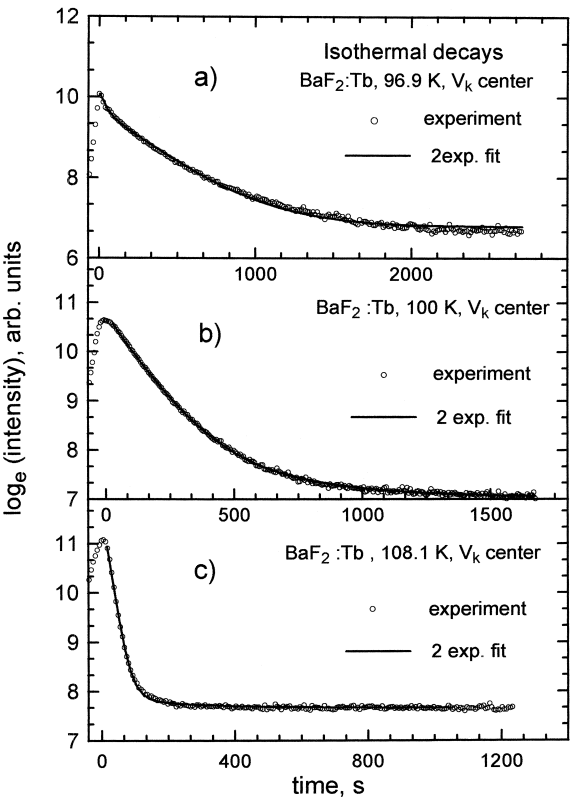

Fig. 5. Representative ITD curves of BaF_2:Tb measured in the vicinity of the V_k glow peak at selected temperatures. Empty circles represent experimental points and solid lines depict two-exponential fits.

Table 2
Summary of the results of ITD measurements and fits for BaF_2:Pr at temperatures in the vicinity of the V_k glow peak[a]

Temp. (K)	y_0	A_1	τ_1 (s)	A_2	τ_2 (s)
90.1	1.1	12	250.8	6.0	2464.7
95.0	1.7	113	57.8	23.6	544.9
100.0	0.2	1	126.1	0.3	410.0
104.0	0.2	2	18.4	3.3	71.3
105.0	1.1	76	14.1	20.5	63.15
106.1	0.2	5	26.4	0.4	81.8
108.1	1.3	80	13.9	2.1	123.8

[a] Decay times (s) and zero-time amplitudes (arb. units) represent parameters extracted from two-exponential fits to the experimental points.

Table 3
Summary of the results of ITD measurements and fits for BaF_2:Tb at temperatures in the vicinity of the V_k glow peak[a]

Temp. (K)	y_0	A_1	τ_1 (s)	A_2	τ_2 (s)
90.1	0.9	31	119.9	1.6	1090.3
95.0	0.8	2	93.0	3.6	667.2
96.9	0.9	8	36.6	15.1	346.7
100.0	1.1	33	123.3	3.8	344.2
104.0	1.0	25	22.3	1.4	68.7
108.1	2.1	53	21.1	0.6	195.8

[a] Decay times (s) and zero-time amplitudes (arb. units) represent parameters extracted from two-exponential fits to the experimental points.

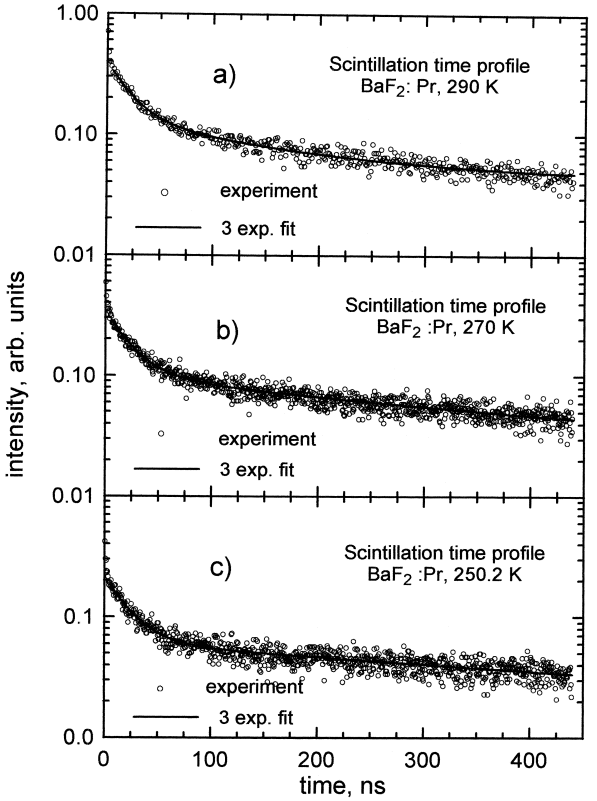

Fig. 6. Representative scintillation time profiles of BaF_2:Pr measured at different temperatures under γ-excitation. Note the fast (20 ns, d–f) and the slow components in the profiles. The slow component decay time depends upon temperature (see text).

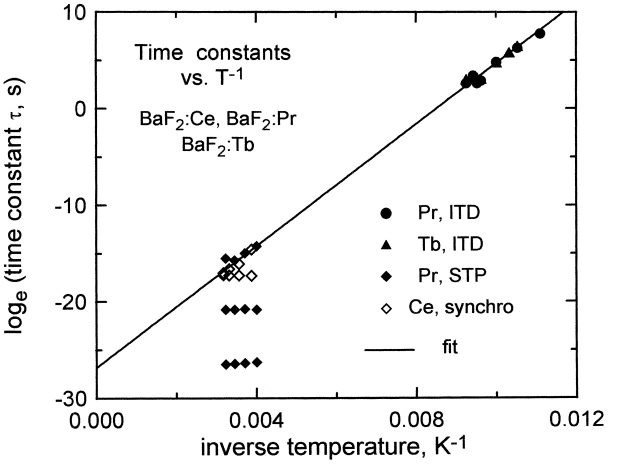

Fig. 7. Trap lifetimes against the inverse temperature. Points in the diagram were obtained from fits to decays measured in three different experiments (isothermal decays, scintillation time profiles under γ-, and photoluminescence time profiles under synchrotron excitation) for three different samples, BaF_2:Pr (filled circles, ITD; filled diamonds, STP), BaF_2:Tb (filled triangles, ITD) and BaF_2:Ce (empty diamonds, synchro decays). The solid line depicts a straight line fit obtained for selected points (filled circles, triangles and those filled and empty diamonds that show temperature dependence).

decay time constants against the inverse temperature, T^{-1}, as shown in Fig. 7 by filled circles (BaF_2:Pr) and triangles (BaF_2:Tb). Although ITD curves are not truly single-exponential as expected, there is, nevertheless, a dominant component in each of the cases that was chosen as the appropriate one. Also included in the diagram shown in Fig. 7 are the decay time constants found from fits to the scintillation time profiles of BaF_2:Pr (filled diamonds). By empty diamonds we show the decay time constants found from the fits to the synchrotron excited time profiles of BaF_2:Ce.

Note the three sets of points shown in Fig. 7 that represent temperature independent time constants; they reflect the radiative lifetimes of the d–f emissions from Ce^{3+} and Pr^{3+}, and of the CVL transition at 220 nm. Interestingly, the remaining points fall on the straight line and have been, therefore, included into the fit described by the Eq. (3) and shown by a solid line. The fit yields the following values of the parameters; $E = 0.272$ eV, $s = 4.49 \times 10^{11}$ s^{-1}. There is some discrepancy between these values and those obtained previously by Glodo et al. [5]. The possible explanation is that the assignment of the STP and ITD points in their paper is not right. The correct assignment would be to include the STP points of the a trap and ITD points of the a trap to one set of points corresponding to only one trap instead of two different traps as they assumed.

Table 4
Summary of the results and fits of scintillation time profile measurements for BaF_2:Pr at various temperatures[a]

Temp. (K)	y_0	A_1	τ_1 (ns)	A_2	τ_2 (ns)	A_3	τ_3 (ns)
310	6.38	681	0.92	79	23.6	26	189.7
290	4.26	271	0.93	28	20.6	10	154.8
270	2.26	222	0.98	25	22.4	8	330.5
250	0.20	167	0.93	17	22.3	6	688.0
220	2.39	138	0.91	16	18.5	2	186.4
200	2.03	103	0.94	11	20.5	2	72.5
180	0.87	64	0.91	6	21.4	1	188.1
160	0.62	45	0.88	5	18.2	1	202.8
140	0.33	14	0.98	1	31.8	0.4	146.8
120	0.30	9	1.04	0.9	22.1	0.2	189.1
100	0.03	5	1.34	0.5	23.9	0.3	1137.3
80	0.08	4	1.08	0.3	22.0	0.2	1195.9
60	0.07	3	1.05	0.3	21.8	0.07	1275.3

[a] Decay times (ns) and zero-time amplitudes (arb. units) represent parameters extracted from three-exponential fits to the measured profiles.

3.5. Scintillation light yield against temperature

In Fig. 8 we show the results of scintillation light yield measurements on BaF_2:Pr against the temperature for a shaping time of 0.5 μs. Each of the experimental points shown in this Fig. gives an integrated amount of scintillation light produced in one event in which one γ-photon

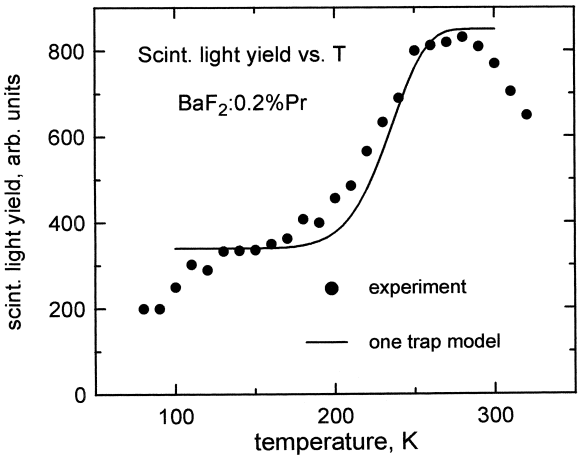

Fig. 8. Scintillation light yield of BaF_2:Pr against temperature for a shaping time of 0.5 μs. Experimental points shown by filled circles reflect the positions of photopeaks obtained under γ-excitation at various temperatures. The solid line was calculated from a one trap model (see text) with trap parameters obtained from the fit shown in Fig. 7. The only parameters varied were the branching coefficients (the direct, *a*, is 0.4 and trap related, *b*, is 0.6 of the total light yield).

was stopped. The solid line was calculated according to the following formula discussed in Ref. [3]:

$$\mathrm{LY} = \mathrm{LY}_0 \left\{ a + b \frac{\tau_{\mathrm{rad}}}{\tau_{\mathrm{rad}} - \tau} \times \left[1 + \frac{\tau}{\tau_{\mathrm{rad}}} \left[\exp\left(-2.35 \frac{\tau_{\mathrm{sh}}}{\tau} \right) - 1 \right] \right] \right\} \quad (4)$$

where LY_0 is the LY (light yield) of the 'trap-free' material, τ_{rad} is the radiative lifetime and τ is, as in (2) and (3), the trap lifetime. Note that except for the branching coefficient *a* (equal to 0.4) and *b* (0.6) that describe contributions from direct and trap mediated recombination routes via the emitting center, there were no other parameters varied to obtain a good fit. The agreement is reasonably good.

4. Conclusions

The three rare earth ions, Ce, Pr and Tb, doped into the host of BaF_2, are potentially interesting in applications such as solid state radiation detectors or X-ray phosphors. In the wavelength range of interest in those applications these ions exhibit d–f (Ce^{3+}), d–f and f–f (Pr^{3+}) and f–f (Tb^{3+}) emissions under selective excitation by light of an appropriate wavelength. Under the X-ray excitation all of these emissions are present but there are also the STE and CVL emissions that are characteristic of the undoped BaF_2 host. These latter emissions represent competitive processes that divert some of the energy deposited in the host material by an ionizing radiation away from the rare earth ion activators and should be minimized.

The winner among the three activator rare earth ions we have studied in this work is clearly the Ce^{3+} ion. This ion supports two recombination channels, one of which involves efficient hole trapping (creating Ce^{4+}) followed by electron trapping and d–f emission (a direct component). Let us note that, quite remarkably, the hole trapping by Ce^{3+} ions must compete successfully with the process of self-trapping as the intensity of the STE emission is clearly diminished upon Ce-doping. The second mode of recombination involves electron trapping by Ce^{3+} ions (creating Ce^{2+} and/or PC centers involving Ce) and a subsequent thermally activated process of V_k release, diffusion and recombination. This mode also contributes to the Ce^{3+}d–f emission although the relevant scintillation component is slower and temperature dependent.

The Pr^{3+} doping does not prevent a large (and undesired) contribution from the radiative decay of self-trapped excitons. Despite that it seems that the Pr^{3+}d–f emission bands observed in the radioluminescence spectra of BaF_2:Pr are due to the first of the two recombination channels identified in the previous case of Ce^{3+}. The mere presence of these bands as well as the presence of the fast scintillation component decaying with the Pr^{3+} radiative lifetime of about 20 ns prove that not all of the holes generated by an ionizing radiation self-trap. A significant fraction of these holes is captured by the Pr^{3+} ions. The second mode is less likely to feed efficiently the higher lying d-levels of the Pr^{3+} ion as the energy released through the recombination of the Pr^{2+} and V_k is strongly reduced by the V_k relaxation energy. This route will, nevertheless, feed efficiently the lower lying f-levels that are, therefore, contributing strongly to the radioluminescence and scintillation of BaF_2:Pr in proportions much higher than those defined by a cascade process involving d- and f-levels of the Pr^{3+} ion. We note that only the second mode of recombination involves hole self-trapping and detrapping. It must be, therefore, responsible for a significant fraction of the scintillation light generated by γ-particles at room temperature and collected within a time window defined by a shaping time of 0.5 μs.

Interestingly the Tb^{3+} doped BaF_2 under X-irradiation shows only little contribution of the STE emission despite the fact that f–d absorptions do not appear to overlap the STE emission band. Therefore the STE-Tb^{3+} energy transfer is not very likely and the only way in which the energy deposited in the BaF_2 host by ionizing radiation can be transferred to Tb^{3+} ions is by a hole and subsequent electron trapping and recombination at the Tb^{3+} sites. The well known strong tendency of Tb^{3+} toward the stable 4+ charge state that would promote the first mode of recombination via Tb^{3+} is clearly consistent with the little contribution from the STEs observed in the radioluminescence. On the other hand the (much smaller) thermoluminescence and ITD curves from the V_k glow peak suggest that also the second channel of recombination via Tb^{3+} is active. We conclude that although the Tb^{3+} ion in BaF_2 does not

show fast d–f emissions and is not appropriate for fast scintillation detector materials, the total steady state radioluminescence output can be very high.

The general conclusion of this work is that recombination of charge carriers (not necessarily band charge carriers) through the rare earth ion activators in BaF_2 is likely to provide the basic light producing mechanism under ionizing irradiation. The presence of intrinsic or extrinsic defects generated (or activated) by ionizing irradiation is likely to interfere with the scintillation process by diverting part of the energy deposited in the host into slower components. Therefore both the scintillation light yield and scintillation time profiles are likely to be affected.

Acknowledgements

This work was supported by the Committee for Scientific Research (KBN) of Poland under the grant no 2P03B04914, by the TMR-Contract ERBFMGECT950059 of the European Community, by the US Department of Energy (grant no DE-FG02-96-ER82117 and DE-FG-02-90-ER61033) and by ALEM Associates, Boston. We are also very grateful to Professor G. Zimmerer and Dr. M. Kirm of HASYLAB, Hamburg, Germany, for their hospitality and help in VUV experiments.

References

[1] K. Meijvogel, A.J.J. Bos, P. Dorenbos, C.W.E. van Eijk, in: P. Dorenbos, C.W.E. van Eijk (Eds.), Proc. Int. Conf. on Inorganic Scintillators and Their Applications, SCINT95, Delft 1995, Delft University Press, Delft, 1996.
[2] A.J. Wojtowicz, W. Drozdowski, D. Wisniewski, K.R. Przegietka, H.L. Oczkowski, T.M. Piters, Rad. Meas. 29 (1998) 323.
[3] A.J. Wojtowicz, J. Glodo, W. Drozdowski, K.R. Przegietka, J. Lumin. 79 (1998) 275.
[4] A.J. Wojtowicz, Acta Phys. Pol. A 95 (1999) 165.
[5] J. Glodo, P. Szupryczynski, A. J Wojtowicz, Acta Phys. Pol. A95 (1999) 259.
[6] A.J. Wojtowicz, W. Drozdowski, J. Glodo, D. Wisniewski, Hasylab Annual Report ‘98, Hamburg, 1999.
[7] R. Visser, P. Dorenbos, C.W.E. van Eijk, A. Meijerink, G. Blasse, H.W. den Hartog, P. Phys.: Condens. Matter 5 (1993) 1659.
[8] W. Hayes, Crystals with the Fluorite Structure, Clarendon Press, Oxford, 1974.
[9] G. Zimmerer, Nucl. Instr. Meth. Phys. Res. A 308 (1991) 178.
[10] http://www-hasylab.desy.de/facility/experimental_stations/stations/; see the I-beamline.
[11] J.H. Beaumount, W. Hayes, D.L. Kirk, G.P. Summers, Proc. Roy. Soc. Lond. A 315 (1970) 69.
[12] J.T. Randall, M.H.F. Wilkins, Proc. Roy. Soc. Lond. A 184 (1945) 366.